# Laminar and Turbulent Flow Calculations for the HIFiRE-5b Flight Test

Kevin M. Porter*, Jonathan Poggie†
*Purdue University, West Lafayette, IN 47907-2045, USA*
and
Roger L. Kimmel,‡§
*Air Force Research Laboratory, Wright-Patterson Air Force Base, OH 45433, USA*

**The HIFiRE-5b program launched an experimental flight test vehicle to study laminar-turbulent transition at hypersonic speeds. To correctly interpret the data collected from the flight, the local atmospheric conditions and the speed and attitude of the vehicle through its trajectory are required. To this end, laminar and turbulent flow calculations were carried out for a range of conditions that bounded the flight conditions. The computed surface pressure and heat transfer were compared to values measured in flight to obtain a best estimate of vehicle attitude and flow conditions. Here we present a summary of those calculations, and a computational database for processing the flight measurements. The final product of this work is an interpolant for heat transfer and pressure in the following variables: angle-of-attack, yaw angle, Mach number, Reynolds number, circumferential station, and streamwise station.**

## I. Introduction

The Hypersonic International Flight Research Experimentation Flight Test 5b (HIFiRE-5b) was a refly in May 2016 of the HIFiRE-5 flight test that occurred in April 2012.[1] Both tests were intended to investigate hypersonic laminar-turbulent transition, but hardware problems with HIFiRE-5 limited that test to a Mach number of about 3. The HIFiRE-5b flight successfully reached a Mach number of over 7.8, and is the subject of the present work.

In order to analyze the HIFiRE-5b transition experiment, the vehicle attitude must be known accurately as a function of flight time. Vehicle attitude was determined post flight by integrating the acceleration in each direction obtained with at set of accelerometers, then comparing the calculated data to the trajectory provided by a Global Positioning System receiver.[2,3] Because the attitude is determined by integration over time, the data are susceptible to accumulation of error during the flight. This error is especially important for HIFiRE-5b, where the primary experiment took place well into the flight. Therefore another method of determining attitude is desirable to ensure that the best possible estimate of the flight conditions is used in the data analysis. An alternative method of determining attitude uses the pressure and heat transfer data obtained during the flight from onboard sensors, along with the results of numerical simulations, to back out a best estimate of the conditions along the trajectory.

In the present study, fully laminar and fully turbulent flow calculations were carried out for a range of conditions that bounded the flight conditions. The computed surface pressure and heat transfer were compared to values measured in flight to obtain a best estimate of vehicle attitude, Mach number, and Reynolds number. Here we present a summary of those calculations, and a computational database for processing the flight measurements. The final product of this work is an interpolant for heat transfer and pressure in

*Graduate Student, School of Aeronautics & Astronautics, Member AIAA
†Associate Professor, School of Aeronautics & Astronautics, Associate Fellow AIAA
‡Principal Aerospace Engineer, AFRL/RQHF, Associate Fellow AIAA

the following variables: angle-of-attack, yaw angle, Mach number, Reynolds number, circumferential station, and streamwise station.

Additional analysis of the HIFiRE-5b transition experiment is presented in companion papers.[4–8] In particular Jewell et al.[6] and Juliano et al.[7] make use of the present calculations.

## II. Procedure

The HIFiRE-5b test article was a blunt 2:1 elliptic cone, 0.861 m long, with a 7 deg minor-axis half-angle and a 2.5 mm minimum nose radius. The simulated configuration is shown in Fig. 1. This configuration has been the subject of a number of previous studies,[9–15] and serves as a simple configuration for investigating the effects of basic-state three-dimensionality on hypersonic laminar-turbulent transition, with a shape representative of a production hypersonic vehicle. Also shown in the figure are the sign conventions for the vehicle attitude, Fig. 1(c), and the sensor locations on the flight test vehicle, Fig. 1(d). In the present study, fully laminar and fully turbulent flow calculations were carried out for the elliptic cone for a range of conditions that bounded the flight conditions for the time around the primary transition experiment.

The computations were carried out using Overflow, an structured, overset grid solver developed by NASA.[16] Standard options were used for the calculations with Overflow. For the turbulent calculations, the Spalart-Allmaras model (SA-noft2) was employed. The right-hand-side used central difference Euler terms, and the left-hand-side used the SSOR algorithm with subiterations.

For each case, grid sequencing, with two refinement steps, was employed to accelerate convergence. The CFL control was was set to a minimum of 0.05 and a maximum of 1.0. The cases were run until the residuals stopped changing and were deemed to be small enough to consider the case to be converged, typically around $1.0 \times 10^{-13}$. Converged solutions were typically obtained after $\sim 10^5$ iterations.

An overset grid system was used for the computations to avoid a singular line in the nose region that would have been present if a single block topology had been used. There were two grid domains. One grid blanketed the region near the nose of the body, and will be called the cap grid here. The second grid represented the region farther downstream, and will be called the body grid.

The computational mesh is illustrated in Fig. 2, which corresponds to the turbulent, final case in Table 1. The figures on the left, Figs. 2(a), 2(c), and 2(e), show the body grid from different perspectives, and the figures on the right, Figs. 2(b), 2(d), and 2(f), show the corresponding views for the cap grids.

A custom algebraic grid generation program was developed to allow fine control in the adjustment of the grid parameters. The program also allowed for the possibility of creating very large grids for direct numerical simulation or implicit large-eddy simulation in the future. Grid clustering was employed near the body surface to accurately capture the wall heat transfer, and the grid was approximately aligned with the bow shock. The generated grids were passed through the NASA program Pegasus[17] to obtain the connectivity information for interpolation in Overflow.

## III. Results

Calculations were carried out with the NASA code Overflow[16] for fully laminar flow and fully turbulent flow. The reference conditions were a freestream Mach number of $M_\infty = 7.7$ and a Reynolds number, based on the minimum nose radius of $R = 2.5$ mm, of $\mathrm{Re}_R = 12500$. The corresponding unit Reynolds number was $5.0 \times 10^6$ m$^{-1}$. The freestream temperature was 221 K and the wall temperature was 373 K. Additional runs were carried out in the range $7.7 \leq M_\infty \leq 8.0$, $12500 \leq \mathrm{Re}_R = 50000$, $0.0^\circ \leq \alpha \leq 2.0^\circ$, and $0.0^\circ \leq \beta \leq 2.0^\circ$.

A conventional grid resolution study was carried out for the mesh parameters listed in Table 1. The same set of grids was employed for both the laminar and turbulent cases. The initial coarse grid consisted of about $1.7 \times 10^6$ points, including both the cap and body domains. Medium and fine grids of $1.3 \times 10^7$ and $1.0 \times 10^8$ points, respectively, were generated by successively doubling the number of cells in each direction with the form of the distribution of points held fixed.

The wall heat flux is a challenging test of grid convergence, and one of the main parameters of interest in the present study. Calculations were carried out for the baseline flow conditions for a laminar flow and a turbulent flow case with an angle-of-attack of $\alpha = 2^\circ$ and a yaw angle of $\beta = 2^\circ$.

The laminar flow results are presented in Fig. 3, which shows the Stanton number as a function of angle around the vehicle circumference for two streamwise stations: $x = 0.40$ m and $x = 0.82$ m. These stations were chosen to correspond with those of sensors used in the flight test; see Fig. 1(d). Note that an

asymmetrical distribution is expected here because of the finite values of the angle-of-attack and the yaw angle. Excellent grid convergence is seen for the heat transfer peaks near the leading edges ($\phi = \pm 90°$). A difficulty appears on the top and bottom of the model ($\phi = 0°$ and $\phi = 180°$): here additional grid resolution leads to the appearance of more peaks in the heat transfer distribution. We believe that this behavior reflects the resolution of stationary instabilities of the three-dimensional flow as the grid becomes finer. It may not be possible to obtain a strictly laminar basic state on a very fine grid.

A basic state solution was desired for the laminar flow calculations, and the oscillations observed in Fig. 3 were judged to be undesirable for this purpose. Thus, the production laminar flow runs were carried out on a mesh that was selectively coarsened from the medium grid case. This is designated the laminar, final case in Table 1.

Better grid convergence is obtained for the turbulent flow cases, which are shown in Fig. 4. The coarse grid is already close to grid convergence, and the results for the medium and fine grids are essentially indistinguishable. The turbulent flow results are qualitatively similar to the laminar flow results, with high heating near the leading edges and minima on the flat sides of the body. The peak heating rate is about a factor of two higher for the turbulent flow case relative to the laminar flow case.

For the production calculations, the medium grid was judged to be sufficient for the turbulent flow cases. This case is called out in Table 1 as the turbulent, final case.

To illustrate the overall structure of the flow, the density field is shown for two turbulent flow cases in Figs. 5–6.

Figure 5 shows the results for the case $\alpha = 0.0$ deg and $\beta = 0.0$ deg, in side view, Fig 5(a); streamwise view, Fig 5(b); and top view, Fig 5(c). The bow shock is evident as the sharp transition from light blue to red, and the boundary layer appears as a dark blue, low-density region. Note that the shock is stronger near the leading edges because of the larger flow turning angle in that region. One of the striking features of the flow is the distinct thickening of the boundary layer on the upper and lower sides of the body. This feature arises from the strong circumferential pressure gradients, and consequent convergence of the boundary layer toward the flat side of the body.

An analogous set of images is shown in Fig. 6 for the case $\alpha = 2.0$ deg and $\beta = 2.0$ deg. As expected, a distinct asymmetry of the flow is apparent for this case. The shock angles and shock strengths are seen to be different on port vs. starboard and windward vs. leeward sides of the body. Of particular note is the shift in the thickening of the boundary layer off the centerline of the body, Fig. 6(b).

A series of production runs was carried out with variations from a reference condition of $\alpha = 0.0$ deg, $\beta = 0.0$ deg, $M_\infty = 7.7$, and $\mathrm{Re}_R = 12500$.

Figure 7 shows the wall pressure for the baseline conditions for both the laminar and turbulent flow cases. The laminar flow case is shown on the left, and the turbulent case on the right. Here the horizontal axis is the streamwise distance along the cone, and the vertical axis is the unwrapped angle around the circumference. The leading edges correspond to $\phi = \pm 90°$, and the top and bottom centerline to $\phi = 0°$ and $\phi = 180°$, respectively. The results are essentially the same for laminar and turbulent flow. Peak pressure occurs on the cone's leading edge, with a minimum on the top and bottom centerline.

An analogous set of plots of the heat transfer over the body surface are shown in Fig. 8. Again, a prominent feature of the wall heat flux distribution is a strong peak along the vehicle leading edge. The distribution is qualitatively similar for laminar and turbulent flow, with higher values by about a factor of two for the turbulent case.

The sensitivity of the wall heat transfer to vehicle attitude and flow conditions is presented in Fig. 9. With the other variables held fixed, the effects of varying angle-of-attack, yaw angle, Mach number, Reynolds number, and circumferential station are examined in turn. Mach number and Reynolds number are seen to have a moderate effect on heating for the range considered, with a stronger effect of angle-of-attack. The heat transfer distribution is seen to undergo profound changes with variation in $\beta$ and $\phi$ because of the strong changes in flow structure around the circumferential direction.

## IV. Summary and Conclusions

The HIFiRE-5b program launched an experimental flight test vehicle to study laminar-turbulent transition at hypersonic speeds. To correctly interpret the data collected from the flight, the local atmospheric conditions and the speed and attitude of the vehicle through its trajectory are required. To this end, laminar and turbulent flow calculations were carried out for a range of conditions that bounded the flight conditions.

The computed surface pressure and heat transfer were compared to values measured in flight to obtain a best estimate of vehicle attitude and flow conditions. This paper has provided a summary of those calculations, and a computational database for processing the flight measurements.

The computational effort culminated in the production of a set of interpolants that could be used to determine the pressure and heat transfer anywhere on the vehicle for any condition. The interpolants were built using Matlab's `griddedInterpolant` function. Each interpolants had six control variables: Mach number, Reynolds number, pitch angle, yaw angle, circumferential angle, and streamwise distance; and one output variable, either surface pressure or heat transfer. Any combination of these variables could be used to generate the output variable by way of a spline function interpolation. Separate interpolants were created for the laminar and turbulent cases.

## Acknowledgments

This project was funded in part by the Air Force Office of Scientific Research, under a grant monitored by I. Leyva, AFOSR/RTE. K. Porter and J. Poggie received support under the Air Force Research Laboratory Summer Faculty Fellowship Program. The Air Force Research Laboratory Department of Defense Supercomputing Resource Center provided computer time. The authors are indebted to D. Garmann and N. Bisek for help in carrying out the computations.

## References

[1]Juliano, T. J., Adamczak, D., and Kimmel, R. L., "HIFiRE-5 Flight Test Results," *Journal of Spacecraft and Rockets*, Vol. 52, No. 3, 2015, pp. 650–663.

[2]Jewell, J. S., Miller, J. H., and Kimmel, R. L., "Correlation of HIFiRE-5 Flight Data With Computed Pressure and Heat Transfer," AIAA paper 2015-2019, June 2015.

[3]Jewell, J. S., Miller, J. H., and Kimmel, R. L., "Correlation of HIFiRE-5a Flight Data with Computed Pressure and Heat Transfer," *Journal of Spacecraft and Rockets*, 2017, accepted for publication.

[4]Kimmel, R. L., Adamczak, D. W., and DSTG AVD Brisbane Team, "HIFiRE-5b Flight Overview," AIAA paper, June 2017, presented at AIAA Aviation 2017, paper number to be assigned.

[5]Borg, M. P. and Kimmel, R. L., "Ground Test Measurements of Boundary-Layer Instabilities and Transition for HIFiRE-5 at Flight-Relevant Attitudes," AIAA paper, June 2017, presented at AIAA Aviation 2017, paper number to be assigned.

[6]Jewell, J. S., Kimmel, R. L., Poggie, J., Porter, K. M., and Juliano, T. J., "Correlation of HIFiRE-5b Flight Data With Computed Pressure and Heat Transfer for Attitude Determination," AIAA paper, June 2017, presented at AIAA Aviation 2017, paper number to be assigned.

[7]Juliano, T. J., Poggie, J., Porter, K. M., Jewell, J. S., Kimmel, R. L., and Adamczak, D. W., "HIFiRE-5b Heat Flux and Boundary-Layer Transition," AIAA paper, June 2017, presented at AIAA Aviation 2017, paper number to be assigned.

[8]Tufts, M. W., Gosse, R., and Kimmel, R. L., "PSE Analysis of Crossflow Instability on HIFiRE-5b Flight Test," AIAA paper, June 2017, presented at AIAA Aviation 2017, paper number to be assigned.

[9]Schmisseur, J. D., Schneider, S. P., and Collicott, S. H., "Receptivity of the Mach-4 Boundary-Layer on an Elliptic Cone to Laser-Generated Localized Freestream Perturbations," AIAA Paper 1998-0532, January 1998.

[10]Kimmel, R. L., Poggie, J., and Schwoerke, S. N., "Laminar-Turbulent Transition in a Mach 8 Elliptic Cone Flow," *AIAA Journal*, Vol. 37, No. 9, 1999, pp. 1080–1087.

[11]Poggie, J., Kimmel, R. L., and Schwoerke, S. N., "Traveling Instability Waves in a Mach 8 Flow over an Elliptic Cone," *AIAA Journal*, Vol. 38, No. 2, 2000, pp. 251–258.

[12]Choudhari, M., Chang, C.-L., Jentink, T., Li, F., Berger, K., Candler, G., and Kimmel, R., "Transition Analysis for the HIFiRE-5 Vehicle," AIAA Paper 2009-4056, June 2009.

[13]Holden, M. S., Wadhams, T. P., MacLean, M., and Mundy, E., "Review of Studies of Boundary Layer Transition in Hypersonic Flows over Axisymmetric and Elliptic Cones Conducted in the CUBRC Shock Tunnels," AIAA Paper 2009-0782, January 2009.

[14]Gosse, R., Kimmel, R. L., and Johnson, H. B., "CFD Study of the HIFiRE-5 Flight Experiment," AIAA Paper 2010-4854, June 2010.

[15]Juliano, T. J. and Schneider, S. P., "Instability and Transition on the HIFiRE-5 in a Mach-6 Quiet Tunnel," AIAA Paper 2010-5004, June 2010.

[16]Buning, P. G., "NASA OVERFLOW CFD Code," `https://overflow.larc.nasa.gov/`, Accessed: 2017-04-10.

[17]Rogers, S. E., Suhs, N. E., Dietz, W. E., Nash, S. M., and Onufer, J. T., "Pegasus 5 Documentation," `https://www.nas.nasa.gov/publications/software/docs/pegasus5/index.html`, Accessed: 2017-04-10.

**Table 1. Size of numerical meshes.**

| Grid | Cap | Body |
|---|---|---|
| Coarse | $126 \times 51 \times 51$ | $126 \times 105 \times 101$ |
| Medium | $251 \times 101 \times 101$ | $251 \times 205 \times 201$ |
| Fine | $501 \times 201 \times 201$ | $501 \times 405 \times 401$ |
| Turbulent, final | $251 \times 101 \times 101$ | $251 \times 205 \times 201$ |
| Laminar, final | $251 \times 75 \times 75$ | $126 \times 105 \times 201$ |

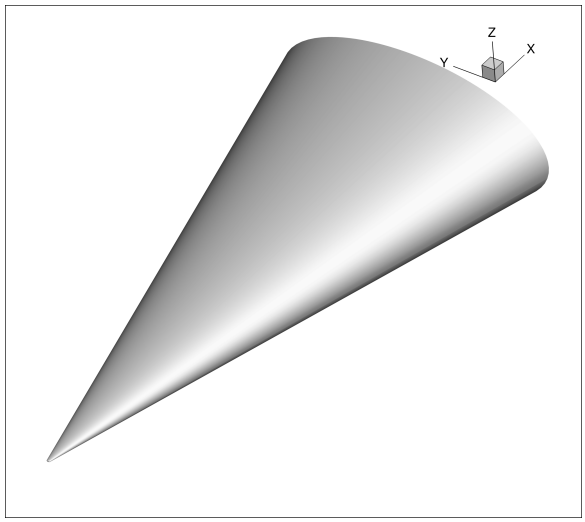


(a) Overview

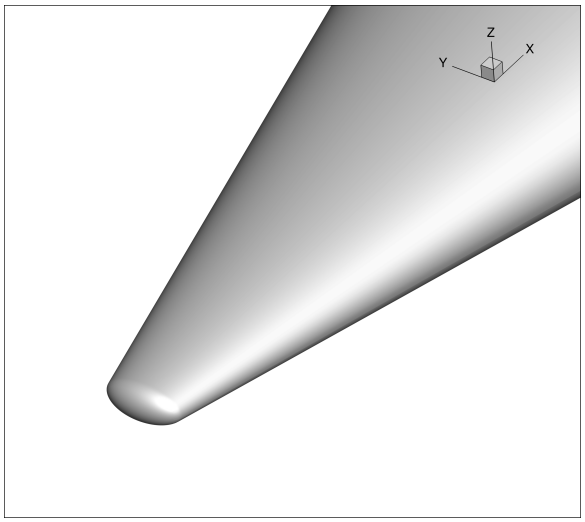


(b) Closeup of nose region

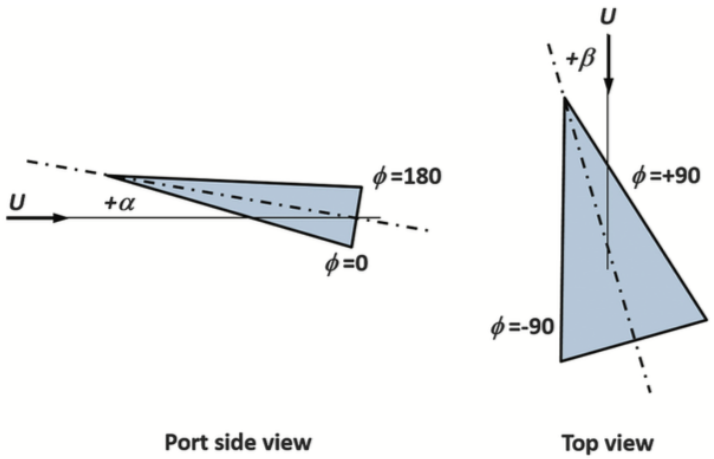


(c) Reference for coordinate system, from Juliano et al.[1]

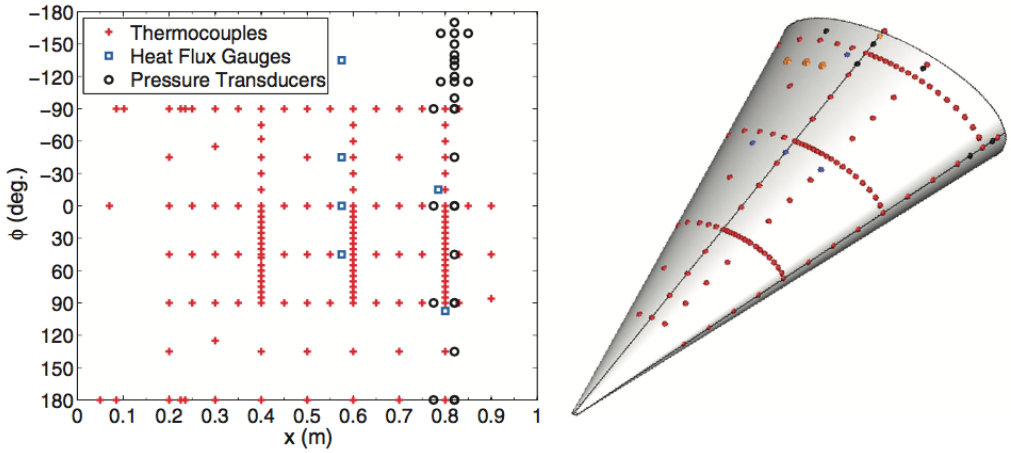


(d) Sensor locations in flight test, from Juliano et al.[1]

**Figure 1. Simulated configuration: HIFiRE-5b test article.**

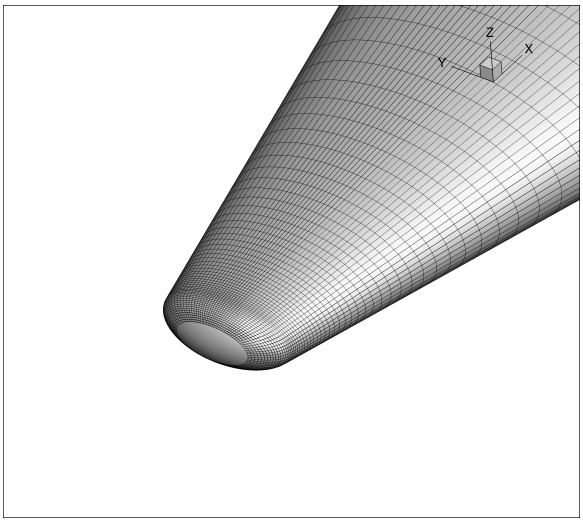


(a) Body region, front view

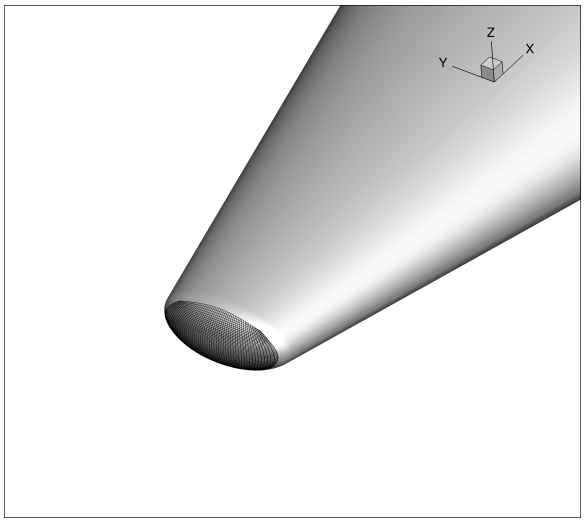


(b) Nose cap, front view

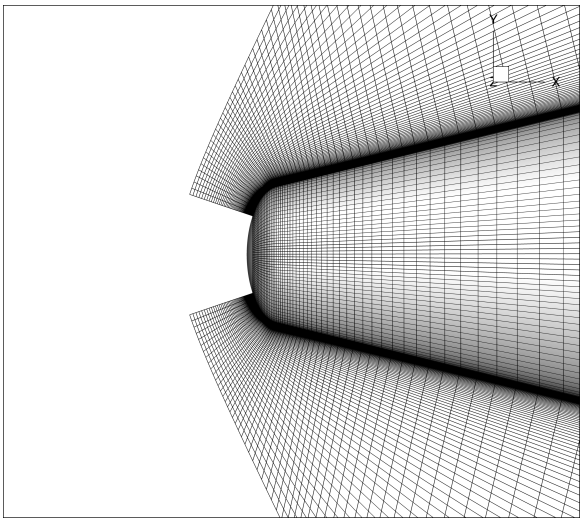


(c) Body region, top view

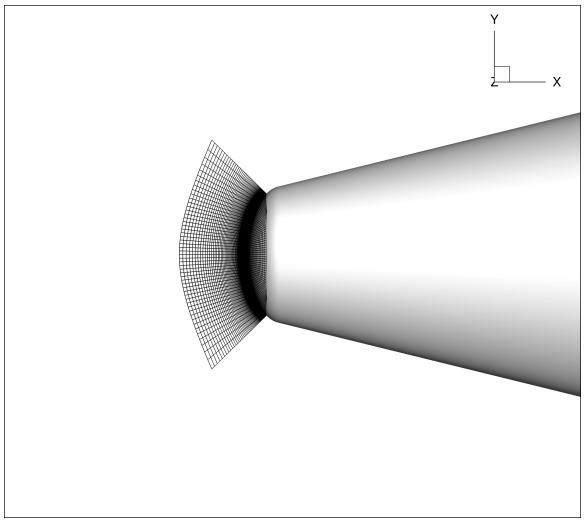


(d) Nose cap, top view

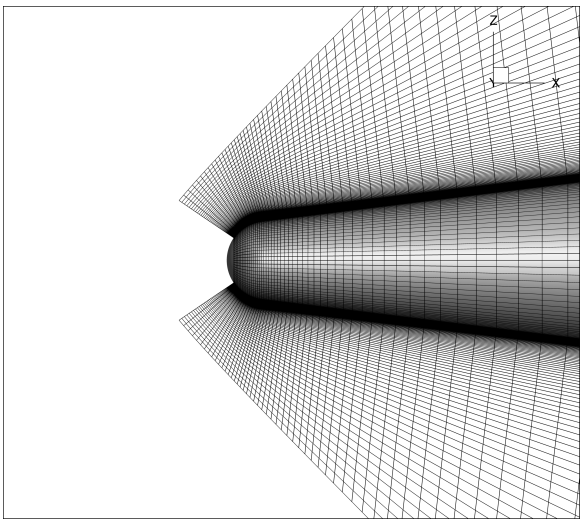


(e) Body region, side view

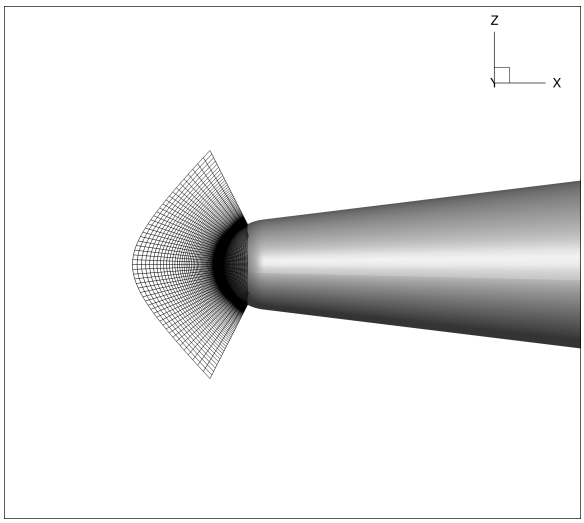


(f) Nose cap, side view

**Figure 2. Computational mesh.**

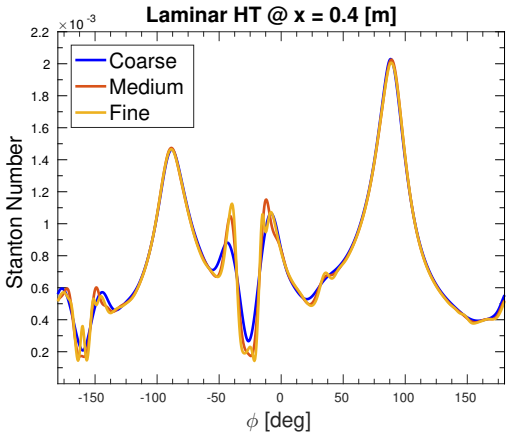


(a) Streamwise station $x = 0.4$ m

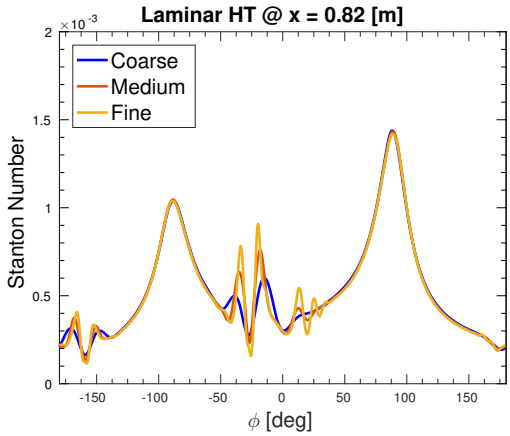


(b) Streamwise station $x = 0.82$ m

**Figure 3. Grid convergence study: laminar heat transfer.**

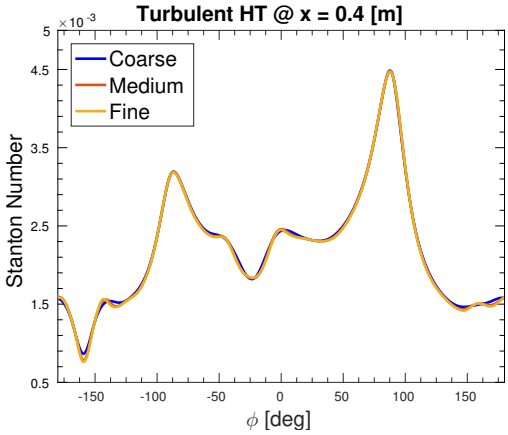


(a) Streamwise station $x = 0.4$ m

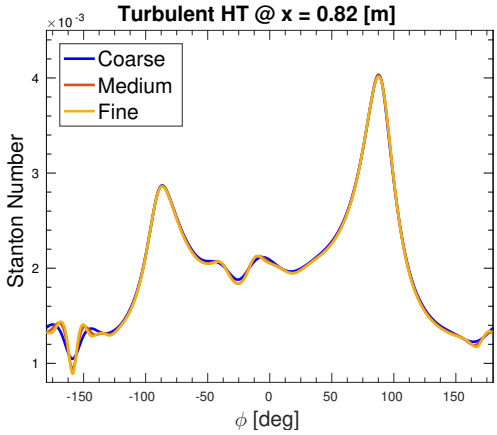


(b) Streamwise station $x = 0.82$ m

**Figure 4. Grid convergence study: turbulent heat transfer.**

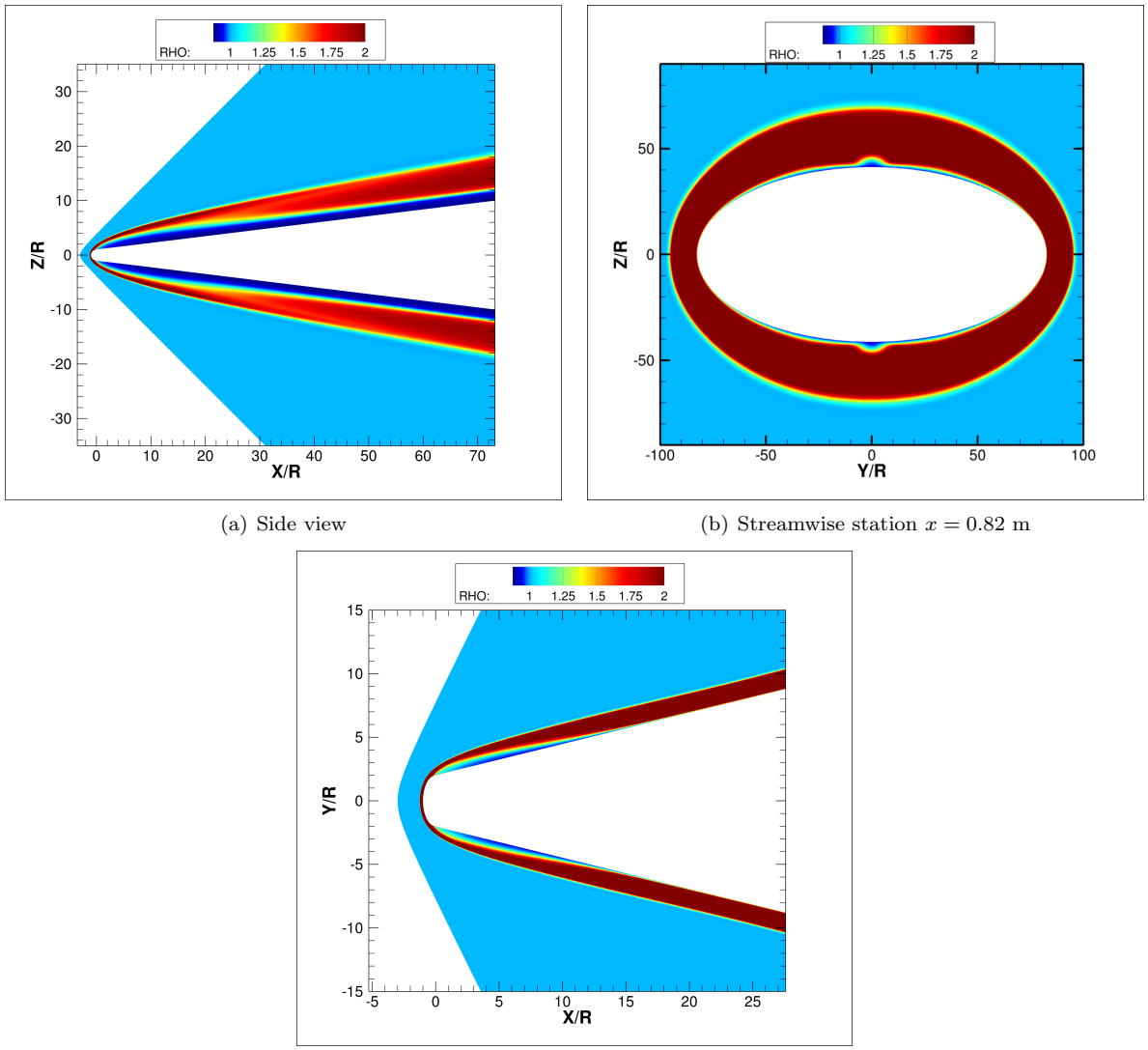


(a) Side view

(b) Streamwise station $x = 0.82$ m

(c) Top view

**Figure 5. Turbulent flow structure: density field at $\alpha = 0.0$ deg and $\beta = 0.0$ deg.**

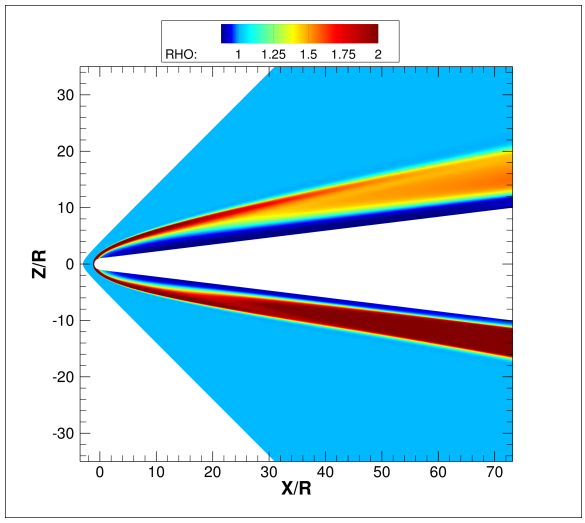


(a) Side view

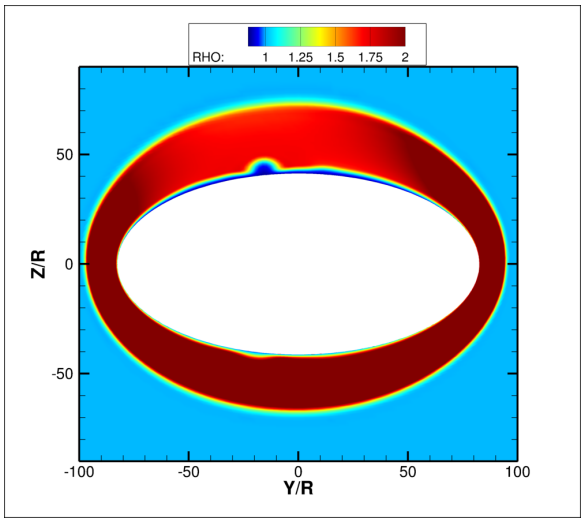


(b) Streamwise station $x = 0.82$ m

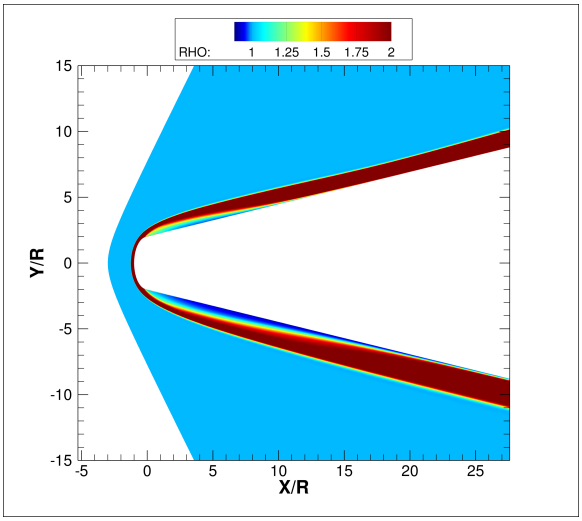


(c) Top view

**Figure 6. Turbulent flow structure: density field at $\alpha = 2.0$ deg and $\beta = 2.0$ deg.**

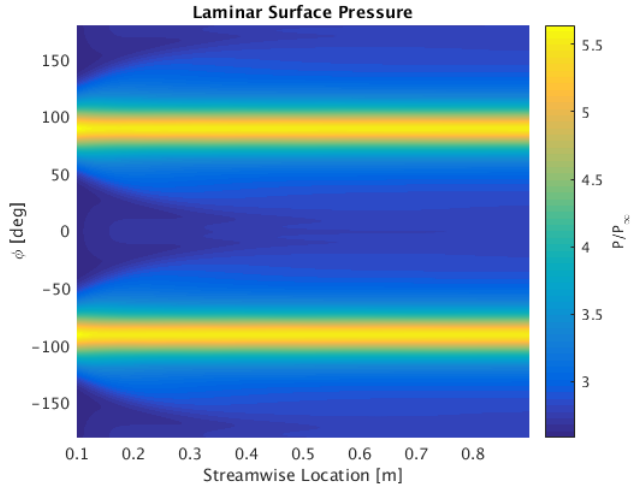


(a) Laminar flow

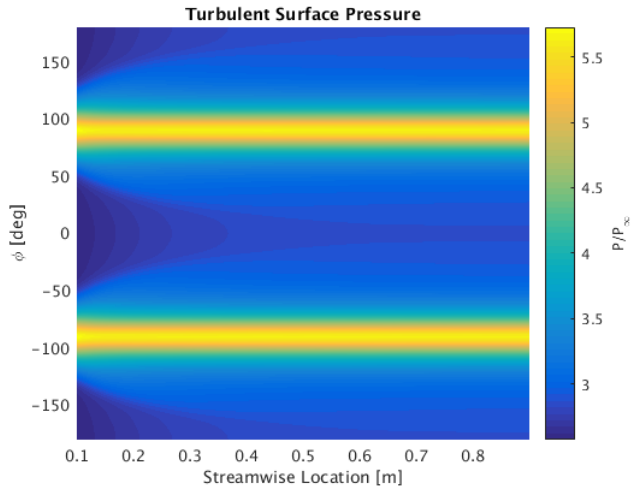


(b) Turbulent flow

**Figure 7. Wall pressure for reference conditions ($\alpha = 0.0$ deg, $\beta = 0.0$ deg, $M_\infty = 7.7$, and $\mathrm{Re}_R = 12500$).**

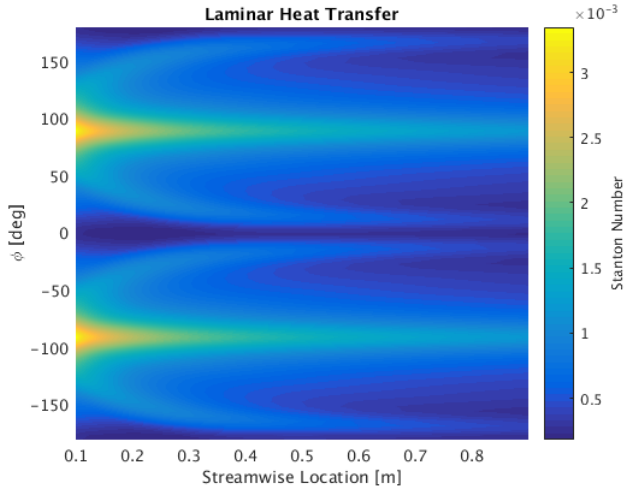


(a) Laminar flow

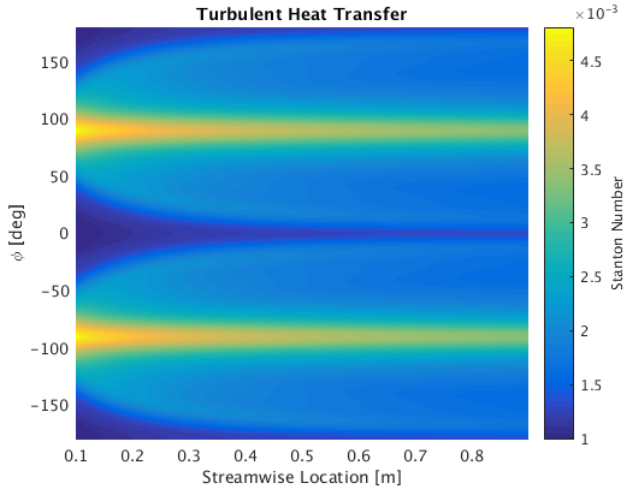


(b) Turbulent flow

**Figure 8. Wall heat transfer for reference conditions ($\alpha = 0.0$ deg, $\beta = 0.0$ deg, $M_\infty = 7.7$, and $\mathrm{Re}_R = 12500$).**

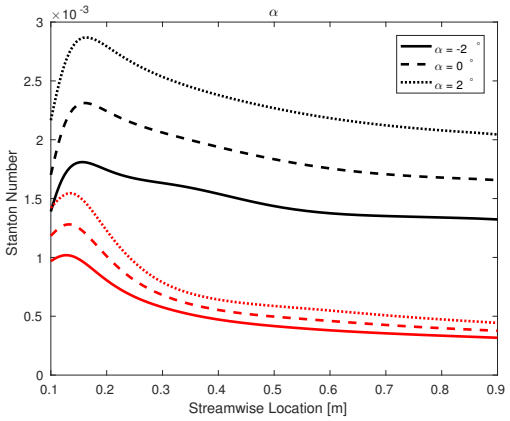


(a) Effect of angle-of-attack

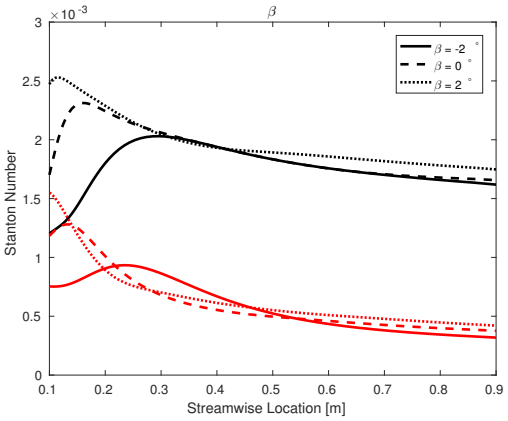


(b) Effect of yaw angle

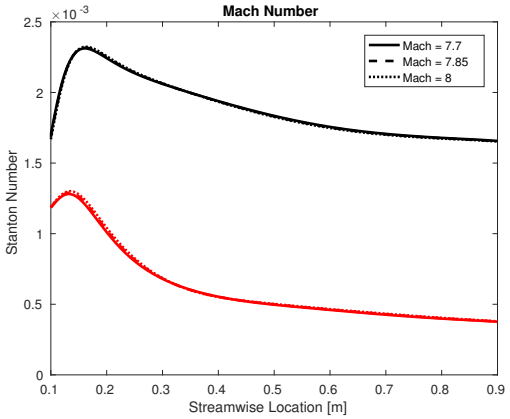


(c) Effect of Mach number

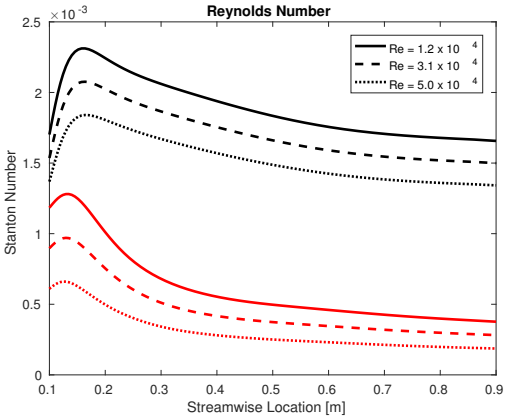


(d) Effect of Reynolds number

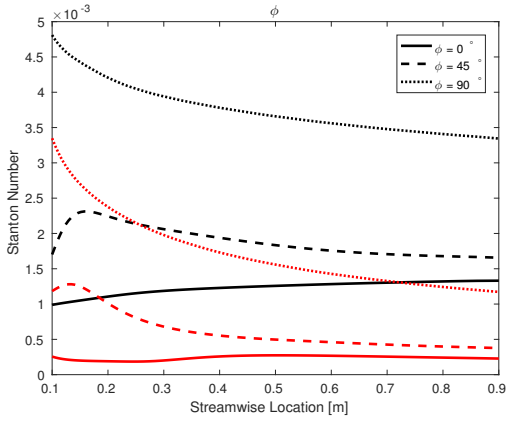


(e) Effect of circumferential station

**Figure 9. Effect vehicle attitude and flow conditions on heat transfer. Unless specified, the reference conditions hold ($\alpha = 0.0$ deg, $\beta = 0.0$ deg, $M_\infty = 7.7$, and $\mathrm{Re}_R = 12500$, $\phi = 45°$ deg). Red lines: laminar flow; black lines: turbulent flow.**